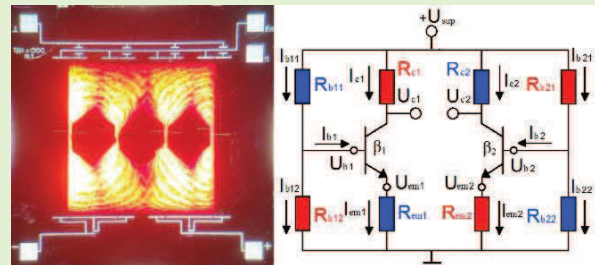


Ultra-High Sensitivity MEMS Pressure Sensor Utilizing Bipolar Junction Transistor for -1...+1 kPa

Mikhail Basov, R&D Engineer

Abstract—The theoretical model and experimental characteristics of ultra-high sensitivity MEMS pressure sensor chip for the range of -1...+1 kPa utilizing a novel electrical circuit are presented. The electrical circuit uses piezosensitive differential amplifier with negative feedback loop (PDA-NFL) based on two bipolar-junction transistors (BJT). The BJT has a vertical structure of n-p-n type (V-NPN) formed on a non-deformable chip area. The circuit contains eight piezoresistors located on a profiled membrane in the areas of maximum mechanical stresses. The circuit design provides a balance between high pressure sensitivity ($S = 44.9$ mV/V/kPa) and fairly low temperature dependence of zero output signal ($TCZ = 0.094\%$ FS/°C). Additionally, high membrane burst pressure of $P = 550$ kPa was reached.

Index Terms—bipolar junction transistor, differential amplifier, piezoresistor, pressure sensor, ultra-high sensitivity.



I. INTRODUCTION

THE development of MEMS pressure sensors has trends similar to well-known vectors in microelectronics. It aimed at chip size reduction while maintaining or improving sensor performance. Chip cost reduction proportional to size reduction allows for expanding the list of applications in the field of medicine, automotive and aviation industries, as well as find new applications in consumer market and HVAC [1]. Reduction of pressure sensitivity is often the price for reduction of chip size for any pressure range. Sensor span often can be considered directly proportional to the membrane area although membrane geometry may put certain restrictions [2]. There are some studies where increase of pressure sensitivity can be obtained by just optimizing the geometry mechanical structure.

For the ultra-low pressure ranges of (0.5-3.0 kPa), pressure sensitivity S with average values above 4-5 mV/V/kPa is required. Pressure sensor chips with area A of 10-25 mm² and profiled membrane with thickness W of thin part in 8-12 μ m range or below is required to meet this requirement. Some mechanical structures can be formed using deep reactive ion etching (DRIE) both from the back side and the front side of the wafer [3-7]. Increasing sensitivity while maintaining chip area on wafer or reducing chip area while maintaining sensitivity for ultra-low pressure ranges requires the membrane thickness reduction and optimization of geometry of mechanical structure for better concentration of mechanical stress (MS). Reducing the membrane thickness often brings

challenges related to wider distribution of parameters of pressure sensors, larger pressure nonlinearity, increase of temperature errors, greater variation of parameters within wafer (especially if etch-stop option is not available for micromachining process), and higher yield loss in volume production, including loss due to damage of thin membranes. The article describes an alternative way to increase the output signal or reduce the size of pressure sensor chips using new stress-sensitive electrical circuit with on-chip signal amplification.

Recently there were several publications on design and modeling of low pressure piezoresistive sensors [8-18]. These publications are mostly focused on achieving higher pressure sensitivity and improving sensor performance by optimization of mechanical structure of pressure sensor chips. Another option for improving pressure sensitivity is related to introducing active elements as transistors to electrical circuit formed on pressure sensor chip. Sensitivity increase due to the use of new electrical circuit utilizing bipolar junction transistor (BJT) at MEMS pressure sensor chip operating for pressure range of -1...+1 kPa is demonstrated. The pressure sensor chip utilizes electrical circuit with BJT-based piezosensitive differential amplifier with negative feedback loop (PDA-NFL). Advantage of the selected electrical circuit relative to classic Wheatstone bridge circuit is in the possibility of combining of a larger number of piezoresistors (PRs) (8 instead of 4) because BJTs are three-pole devices (Fig. 1). The certain combination of nominal values of PRs and their dependence on mechanical stress allows for larger changes of BJT collector potential. The difference between these potentials is used as the circuit output signal. The NFL in electrical circuit allows for reduction of the temperature dependence of the BJT base potential so temperature

12.08.2020.

This work was supported by the Dukhov All-Russia Research Institute of Automatics (VNIIA). (Corresponding author: Mikhail Basov.)
M. Basov is with VNIIA, Moscow 127055, Russian Federation (e-mail: engineerbasovm@gmail.com).

dependence of the output signal can be reduced. If the NFL is absent, then TCZ may be as high as 2.5 %FS/°C and zero thermal hysteresis (THZ) as high as 1.0 %FS [19].

Potentially it is possible to consider sophisticated versions of amplifier circuit with an increased number of BJTs or metal-oxide-semiconductor field effect transistors (MOSFETs) or junction gate field-effect transistors (JFETs) [20-26], as well as with increased number of PR (more than 8 elements). Such development will require:

- Detailed analysis of chip circuit design with effective topological arrangement of active and passive elements within a limited area combined with deep understanding of the physical fundamentals of each circuit component.
- Fabrication process capable of producing chips with well-balanced PDA-NFL circuit. Poor balance of the circuit elements may lead to a significant variability of sensor characteristics.
- Integration of CMOS and MEMS processes, preferably at one manufacturing line.

The main goal of this development is achieving very high pressure sensitivity. The early PDA-NFL chip research [19, 27-29] for the range of -60...+60 kPa showed that the optimized circuit based on n-p-n type BJT (V-NPN) allows for sensitivity increase by 1.54 times relative to the alternative circuit with horizontal p-n-p (L-PNP) BJT. The disadvantage of L-PNP BJT circuit is a parasitic current from emitter of BJT to substrate. At the same time, the circuit with L-PNP transistors demonstrated 4.1 times smaller thermal coefficient of span (TCS) compared to the circuit utilizing vertical V-NPN transistors. In addition, placement of BJTs on a thin portion of membrane was analyzed. This option provides sensitivity increase only by 1-5% but requires much more complex circuit layout because of a small size of areas with high mechanical stress. Therefore, both BJTs have been placed on the non-deformable frame of the chip.

II. MODELING OF ULTRA-HIGH-SENSITIVITY PRESSURE SENSOR PDA-NFL

The mathematical model is based only on piezoresistive effect [29]. The contribution of the piezojunction effect [31–36] is practically insignificant, because BJTs are located on the frame. The membrane structure has three stress-concentrators in form of right islands (RI) formed by wet anisotropic etching (Fig. 2a). Table I presents the geometrical parameters of the ultra-high sensitivity pressure sensor chip PDA-NFL with technological tolerances. Fig. 2b shows stress distribution obtained from ANSYS model utilizing target values of geometrical parameters. Four pairs of PRs are located in four elongated grooves between the RIs (Fig. 2c). Groove width D is 39 μm and groove length Z is 270 μm . The gap between adjacent PRs is 16 μm . The PR width in mask is 10 μm . Each PR is located in area with high stress – either compressive or tensile, depending on the desired change of its nominal value after applying pressure. Target values of resistors R_{b11} , R_{b12} , used as a voltage divider, collector resistors R_{c1} and emitter resistors R_{em1} are different. However, the target values of matching PRs in opposite branch R_{b21} ,

R_{b22} , R_{c2} , R_{em2} are the same. For example, target value of R_{c1} is bigger than R_{c1} but target values of R_{c1} and R_{c2} , R_{c1} and R_{e2} are the same. It is assumed that all resistors formed in a single technological process, have the same p-type doping and the same impurity distribution. The target values of PRs are obtained by changing length of resistors in the mask. When the structure is loaded by pressure $\Delta P = 1$ kPa, then the average von-Mises stress σ in the areas where PRs are located is 21.4 MPa.

In practice shape of RIs may have some variability caused by both deviation of wafer surface orientation from (100) plane and error in mask orientation with respect to $\langle 110 \rangle$ directions [37]. Some asymmetry of RIs was introduced in the model (Fig. 2c) for evaluation of the asymmetry on variability of the output parameters.

The main piezoresistive coefficient for p-type PR (surface concentration $N_S = 8 \cdot 10^{18} \text{ cm}^{-3}$, surface resistance $R_S = 200 \text{ Ohm/cm}^2$, p-n junction depth $x_j = 1.8 \text{ }\mu\text{m}$) at ambient temperature is $\pi_{44} = 1,26 \cdot 10^{-9} \text{ Pa}^{-1}$. This value of π_{44} and target geometrical parameters were used in an idealized mathematical model. The absolute value of relative change of resistance δR for each of eight resistors at applied pressure $\Delta P = 1$ kPa can be evaluated as $\delta R = (\pi_{44} \cdot \sigma)/2 = 1.35 \%$. The nominal values of PRs and operating regimes of BJT were calculated to maximize the ratio between of pressure sensitivity to temperature error. The calculation procedure is quite complex. It is described in detail in [27] for a similar pressure sensor with PDA-NFL designed for pressure range of -60...+60 kPa. Optimum values of resistors, circuit parameters, pressure sensitivity and TCZ calculated using the input parametric values of PDA-NFL electrical circuit presented in Table II.

The modeling results obtained with help of NI Multisim for electrical circuit under applied pressure $\Delta P = 1$ kPa and temperature change by $\Delta T = 10$ °C are shown in Fig. 3a, b. The changes of nominal value of PRs are result of load applied from the cavity side. First circuit branch (left) is presented with changed parameters when the temperature increases by 10 °C ($T_1 = (T_{\text{room}} + 10) \text{ }^\circ\text{C}$) relative room temperature T_{room} and second branch (right) is presented with parameters at room temperature T_{room} to analyze the temperature dependence of PDA-NFL circuit. The operation of Wheatstone bridge circuit with bridge resistance of 4 kOhm under the same stress in the locations of PRs is shown in Fig. 3c. High target gain $\beta = 145$ for BJTs is chosen to minimize the thickness of active base region and reduce the noise of output signal at the same time. The main noise component is Flicker noise caused by carrier generation and recombination effects [38].

The analysis shows the output signal of pressure sensor chip PDA-NFL changes by:

a) $\Delta U_P = 232$ mV under applied pressure $\Delta P = 1$ kPa, which is equivalent to sensitivity $S = 46.4 \text{ mV/V/kPa}$;

b) $\Delta U_T = 2.3$ mV when temperature changes by $\Delta T = 10$ °C. It is equivalent to additional component of temperature error (temperature coefficient of zero signal) $\text{TCZ} = 0.099\% \text{ FS}/^\circ\text{C}$;

c) Pressure sensitivity is 3.5 times higher compared to the output signal of pressure sensor chip with Wheatstone bridge circuit. This result has been also previously experimentally proved on similar samples for higher pressure range of -60...+ 60 kPa [29].

III. EXPERIMENTAL RESULTS OF ULTRA-HIGH SENSITIVITY PRESSURE SENSOR PDA-NFL

Pressure sensor chips were manufactured using (100) p-type Si wafers with n-type epitaxial layer. It is necessary for separating the BJT regions on chip area. Isolation diffusion areas (p^+) extending through full thickness of epi-layer are used to electrically isolate BJTs and PRs. P-type substrate is connected to ground. PRs contain high-doped p^+ -type regions ($N_{sp^+} = 7.4 \cdot 10^{19} \text{ cm}^{-3}$, $x_{jp^+} = 3.6 \text{ } \mu\text{m}$, $R_{sp^+} = 17 \text{ Ohm/cm}^2$) connecting the bond pads located on the frame with low-doped p-type regions described early. The closest metallization region of aluminum with thickness of $0.8 \text{ } \mu\text{m}$ is located at minimum distance of $80 \text{ } \mu\text{m}$ from the thinned part boundary of membrane. It is necessary to reduce negative properties, which were associated with a significant difference between the linear coefficients of temperature expansion for silicon and aluminum.

Although this type of substrates allows for electrochemical etching with etch stop and p-n junction, that option was not used for membrane fabrication. Membranes formed using timed wet etching had significant thickness variation. Consequently, output parameters also had large variation. In further studies, preferably, mechanical structure should have membranes formed using micromachining process with etch stop – either DRIE or wet stop etching [39-45].

Technological route for processing pressure sensor wafers:

1. Oxidation;
2. The sequence of cleaning, photolithography and doping steps, including:
 - a. boron for isolation areas and creating contact to the substrate;
 - b. boron for high-doped PR regions;
 - c. boron for low-doped PR regions and BJT base areas;
 - d. phosphorous for BJT emitter and collector areas;
3. Si_3N_4 deposition as protection layer for membrane etching;
4. Cavity photolithography on the back side of the wafer;
5. Wet anisotropic etching of membrane in 30% KOH aqueous solution at $T = 85 \text{ } ^\circ\text{C}$;
6. Wet isotropic etching of membrane in a mixture of $\text{HF} : \text{HNO}_3 : \text{CH}_3\text{COOH}$ (2:9:4);
7. Removal of Si_3N_4 layer;
8. Photolithography and etching to open contacts;
9. Sputtering of Al-Si (1.5%);
10. Photolithography and metal etching to define metal lines and bond pads;
11. Dicing

Details of diffusion processes are presented in Table III.

The pressure sensor chips (Fig. 4a) were bonded to silicon supports with help of low-temperature glass. Resulting structure, is shown in Fig. 4c. This design allows for hermetic bonding, which is necessary for applying pressure from back side and for reducing of assembly stress (Fig. 4b) [46,47]. The chip works as differential pressure sensing element.

All samples went through temperature cycling and pressure cycling to remove residual assembly stress before testing [48,49]. Characteristics of the samples presented in Table IV. The testing was performed at supply voltage $U_{\text{sup}} = 5.0 \text{ V}$. Sensitivity and related parameters reported from

measurements where pressure was applied from the cavity side. Temperature characteristics were measured in two temperature ranges: from $-30 \text{ } ^\circ\text{C}$ to $+20 \text{ } ^\circ\text{C}$ and from $+20 \text{ } ^\circ\text{C}$ to $+60 \text{ } ^\circ\text{C}$. Overload pressure (proof pressure) testing was done from both sides at 30 kPa . Stability of output signal was tested for 9 hours. The output signal noise was estimated as RMS value of output voltage fluctuation for 20 minutes.

The dependence of output zero signal on temperature for a typical sample is presented on Fig. 5a. Chip analysis shows that BJT enters to saturation mode at a temperature slightly above $T \approx 60 \text{ } ^\circ\text{C}$. Example of output signal noise with respect to its average value (“zero” level) during 20 minutes is shown in Fig. 5b.

IV. DISCUSSION

The ultra-high sensitivity pressure sensor chip PDA-NFL has both advantages and drawbacks, which will require further work.

Advantages:

- The main research target was achieved – the chip with dimensions of $4.0 \text{ mm} \times 4.0 \text{ mm} \times 0.4 \text{ mm}$ for differential pressure range of $-1...+1 \text{ kPa}$ demonstrated high sensitivity of $S = 44.9 \text{ mV/V/kPa}$. The PDA-NFL chip sensitivity is 3.5X times higher than the theoretical value for a chip having similar mechanical structure and utilizing Wheatstone bridge circuit. The similar advantage for pressure range of $-60...+60 \text{ kPa}$ was experimentally proven previously [28, 29].
- The mathematical model for sensitivity and additional component of temperature error analysis showed excellent agreement with experimental data (difference within 5%).
- The high value of burst pressure for this membrane design above $P_{\text{burst}} = 550 \text{ kPa}$ and slight output signal error after overload pressure $P_{\text{proof}} = 30 \text{ kPa}$ were demonstrated.
- The output signal error after flipping sensor in gravity field is identical to signal from applied pressure of 1.4 Pa . The reason for this change is membrane deflection by RI inertial mass.

Disadvantages:

- Sensor temperature errors are high despite using NFL in differential amplifier. Comparative analysis of PDA-NFL circuit and Wheatstone bridge circuit is needed.
- Sensor characteristics have high variation of parameters due to process variation resulting in a wide distribution of membrane thickness and some asymmetry in geometry of rigid islands. It is important to use micromachining process, either DRIE or wet etching, that allows for etch-stop.
- Output signal noise of $60 \text{ } \mu\text{V}$ is significantly higher compared to that for sensors utilizing Wheatstone bridge circuit. This disadvantage can be minimized by using multiple measurements and averaging with help of ASIC. The noise is equivalent to pressure of 1.3 Pa .

- The nonlinearity of output signal typically exceeds 1%. Sensor linearity can be improved by modification of membrane design, including increase length of the grooves between rigid islands. Most likely, relatively large thickness of silicon dioxide layer on thin part of membrane contributes to nonlinearity. Nonuniformity of silicon dioxide thickness due to difference in doping results in additional stress in membrane and may cause a sharp increase of output signal in response to small applied pressure (less than 1 kPa).
- Relatively wide distribution of sensor offset is linked to some imbalance of electrical circuit having two times more passive elements compared to Wheatstone bridge circuit, and variations of BJT parameters. A better balance of differential amplifier circuit will help to achieve better thermal compensation of output signal.

Sensor drift is mainly determined by some instability of the transistors. More work on improvement of sensor stability is needed.

V. CONCLUSION

The Ultra-high sensitivity pressure sensor chips for differential pressure range of $-1...+1$ kPa with on-chip piezosensitive differential amplifier with negative feedback loop (PDA-NFL) manufactured. High average sensitivity of 44.9 mV/V/kPa of the chips, low nonlinearity and temperature errors allows for using them in applications for ultra-low range (1.0 kPa or lower). Approach demonstrated in this development work also allows for a significant chip area reduction for higher pressure ranges. Pressure sensor chip PDA-NFL utilizing vertical NPN bipolar junction transistor (BJT) provides in average 3.5 times higher sensitivity than sensor chip with similar mechanical structure but utilizing Wheatstone bridge circuit. The sensitivity increase due to new electrical circuit allows for manufacturing of membrane structures, which can withstand much higher overload pressure without use of stops in additional assembly elements [50-52].

Described in this paper sensor chip utilizing novel PDA-NFL circuit based on BJTs is a perspective direction for development of advanced piezoresistive sensors. It is expected that temperature errors, pressure nonlinearity and noise can be reduced by optimization of both mechanical structure and electrical circuit.

ACKNOWLEDGMENT

The studies were financially supported by Dukhov All-Russia Research Institute of Automatics.

REFERENCES

- [1] Y. Charentenay, MEMS Pressure Sensor Market and Technologies 2018, I-Micronews. Market & Technology report (2018) 28-31.
- [2] S. Timoshenko, S. Woinowsky-Krieger, Theory of Plates and Shells, MCGraw-Hill, New York, 1970.
- [3] Xu, T., Lu, D., Zhao, L., Jiang, Z., Wang, H., Guo, X., Li, Z., Zhou, X., Zhao, Y., 2017. Application and Optimization of Stiffness Abruption Structures for Pressure Sensors with High Sensitivity and Anti-Overload Ability. *Sensors*. 17, 1965.
- [4] Zhao, L., Xu, T., Hebibul, R., Jiang, Z., Ding, J., Peng, N., Guo, X., Xu, Y., Wang, H., Zhao, Y., 2016. A Bossed Diaphragm Piezoresistive Pressure Sensor with a Peninsula-Island Structure for the Ultra-Low-Pressure Range with High Sensitivity. *IOP Measurement Science and Technology*. 27, 124012.
- [5] Yu, Z., Zhao, Y., Sun, L., Tian, B., Jiang, Z., 2013. Incorporation of Beams into Bossed Diaphragm for a High Sensitivity and Overload Micro Pressure Sensor. *Review Scientific Instruments*. 84, 015004.
- [6] Z. Yu, Y. Zhao, L. Li, C. Li, Y. Liu, B. Tian, Realization of a Micro Pressure Sensor with High Sensitivity and Overload by Introducing Beams and Islands, *Microsyst. Technol.* 21 (2015) 739–747.
- [7] P.K. Kinnell, J. King, M. Lester, R. Craddock, A Hollow Stiffening Structure for Low-Pressure Sensors, *Sensors and Actuators A: Physical* 160 (2010) 35–41.
- [8] L. Li, N. Belov, M. Klitzke, J-S. Park, High Performance Piezoresistive Low Pressure Sensors, *IEEE Sensors Conference* (2016) 1406-1408.
- [9] Tran, A.V., Zhang, X., Zhu, B., 2018. Mechanical Structural Design of a Piezoresistive Pressure Sensor for Low-Pressure Measurement: A Computational Analysis by Increases in the Sensor Sensitivity. *Sensors*. 18, 2023.
- [10] T. Guan, F. Yang, W. Wang, X. Huang, B. Jiang, D. Zhang, The Design and Analysis of Piezoresistive Shuriken-Structured Diaphragm Micro-Pressure Sensors, *Journal of Microelectromechanical Systems* PP(99) (2016) pp. 1-9.
- [11] N. Arjunan, S. Thangavelu, Modeling and Analysis of a Multi Bossed Beam Membrane Sensor for Environmental Applications, *Transactions on Electrical and Electronic Materials* 18 (2017) 25–29.
- [12] Li, C., Cordovilla, F., Jagdheesh, R., Ocana, J.L., 2018. Design Optimization and Fabrication of a Novel Structural SOI Piezoresistive Pressure Sensor with High Accuracy. *Sensors*. 18, 439.
- [13] P. Mackowiak, M. Schiffer, X. Xu, E. Obermeier, H. Ngo, Design and Simulation of Ultra High Sensitive Piezoresistive MEMS Sensor With Structured Membrane for Low Pressure Applications, *12th Electronics Packaging Technology Conference*, (2010) 757-761.
- [14] S. Marco, J. Samitier, O. Ruiz, J.R. Morante, J. Esteved, High-Performance Piezoresistive Pressure Sensors for Biomedical Applications Using Very Thin Structured Membranes, *IOP Measurement Science and Technology* 7 (1996) 1195-1203.
- [15] M. Basov, D. Prigodskiy, Investigation of High Sensitivity Piezoresistive Pressure Sensors at Ultra-Low Differential Pressures, *IEEE Sensors Journal* 20 (2020) 7646-7652.
- [16] M. Basov, D. Prigodskiy, Development of High-Sensitivity Piezoresistive Pressure Sensors for $-0.5...+0.5$ kPa, *Journal of Micromechanics and Microengineering* 30 (2020) 105006.
- [17] J. Wang, X. Xia, X. Li, Monolithic integration of pressure plus acceleration composite TPMS sensors with a single-sided micromachining technology, *Journal of Microelectromechanical Systems* 21 (2012) 284-293.
- [18] C.T. Seo, Y.M. Kim, J.K. Shin, J.H. Lee, A Novel Comb-Type Differential Pressure Sensor with Silicon Beams Embedded in a Silicone Rubber Membrane, *Jpn. J. Appl. Phys.* 43 (2004) 2046–2049.
- [19] M.V. Basov, D.M. Prigodskiy, Investigation of a Sensitive Element for the Pressure Sensor Based on a Bipolar Piezotransistor, *Nano- and Microsystem Technology* 19 (2017) 685-693.
- [20] Hafez, N., Haas, S., Loebel, K., 2018. Characterisation of MOS Transistors as an Electromechanical Transducer for Stress. *Physica Status Solidi A*. 1700680.
- [21] J.M. Sallese, W. Grabinski, V. Meyer, C. Bassin, P. Fazan, Electrical Modeling of a Pressure Sensor MOSFET, *Sensors and Actuators A: Physical* 94 (2001) 53-58.
- [22] Z. Zhang, Y.H. Zhang, L. Liu, T.L. Ren, A novel MEMS pressure sensor with MOSFET on chip, *IEEE Sensors Conference* (2008) 1564-1567.
- [23] R.C. Jaeger, J.C. Suhling, R. Ramani, A. T. Bradley, J. Xu, CMOS stress sensors on [100] silicon, *IEEE Journal of Solid-State Circuits* 35 (2000) 85-95.
- [24] S.I. Kozlovskiy, V.V. Nedostup, I.I. Boiko, First-Order Piezoresistance Coefficients in Heavily Doped P-Type Silicon Crystals, *Sensors and Actuators A: Physical* 133 (2007) 72-81.
- [25] I.G. Neizvestnyi, V.A. Gridchin, The use of stressed silicon in MOS transistors and CMOS structures, *Russian Microelectronics* 38 (2009) 71-86.
- [26] P. Singh, J. Miao, L. Shao, Microcantilever sensors with embedded piezoresistive transistor read-out: Design and characterization, *Sensors and Actuators A: Physical* 171 (2011) 178-185.

- [27] M.V. Basov, D.M. Prigodskiy, D.A. Holodkov, Modeling of Sensitive Element for Pressure Sensor Based on Bipolar Piezotransistor, *Sensors and Systems* 6 (2017) 17-24.
- [28] M. Basov, Development of High-Sensitivity Pressure Sensor with On-chip Differential Transistor Amplifier, *J. Micromech. Microeng.* 30 (2020) 065001.
- [29] M. Basov, High-sensitivity MEMS pressure sensor utilizing bipolar junction transistor with temperature compensation, *Sensors and Actuators A: Physical*, 303, 2020, 111705.
- [30] Y. Kanda, A Graphical Representation of the Piezoresistance Coefficients in Silicon, *IEEE Transactions on electron devices* 29 (1982) 64-70.
- [31] F. Fruett, G.C.M. Meijer, *The Piezjunction Effect in Silicon Integrated Circuits and Sensors*, Springer, Delft, 2002.
- [32] J. Creemer, F. Fruett, G.C.M. Meijer, P.J. French, The Piezjunction Effect in Silicon Sensors and Circuits and Its Relation to Piezoresistance, *IEEE Sens. J.* 1 (2001) 98-108.
- [33] J.C. Doll, B.L. Pruitt, *Alternative Materials and Transduction Methods*, in: *Piezoresistor Design and Applications. Microsystems and Nanosystems*, vol 1., Springer, New York, 2013.
- [34] A.A. Barlian, W.T. Park, J.R. Mallon, A.J. Rastegar, B.L. Pruitt, Review: Semiconductor piezoresistance for microsystems, *Proceedings of the IEEE*, 97 (2009) 513-552.
- [35] D. M. Stefanescu, *Handbook of Force Transducers Principles and Components*, Springer, Berlin, 2011.
- [36] G. G. Babichev, S. I. Kozlovskiy, V. A. Romanov, N. N. Sharan, Silicon pressure transducers with frequency output on base strain sensitive unijunction transistors, *SENSORS*, 2002 IEEE, USA, 2 (2002) 998-1001.
- [37] V. Lindroos, M. Tilli, A. Lehto, T. Motooka, *Handbook of Silicon Based MEMS Materials and Technologies*, William Andrew Applied Science Publishers, Oxford, 2010.
- [38] B.M. Wilamowski, J.D. Irwin, *The industrial Electronics Handbook. Fundamentals of industrial electronics*, Taylor and Francis Group, Boca Raton, 2011.
- [39] R.H. Johnson, S. Karbassi, U. Sridhar, B. Speldrich, A High-Sensitivity Ribbed and Bossed Pressure Transducer, *Sensors and Actuators A: Physical* 35 (1992) 93-99.
- [40] X. Huang, D. Zhang, A High Sensitivity and High Linearity Pressure Sensor Based on a Peninsulastructured Diaphragm for Low-Pressure Ranges, *Sensors and Actuators A: Physical* 216 (2014) 176-189.
- [41] M. Bao, *Analysis and Design Principles of MEMS Devices*, Elsevier Science, Amsterdam, 2005.
- [42] J.R. Mallon, F. Pourahmadi, K. Petersen, P. Barth, T. Vermeulen, J. Bryzek, Low-Pressure Sensors Employing Bossed Diaphragms and Precision Etch-Stopping, *Sensors and Actuators A: Physical* 21 (1990) 89-95.
- [43] H. Sandmaier, K. Kuhl, A square-diaphragm piezoresistive pressure sensor with a rectangular central boss for low-pressure ranges, *IEEE Transactions on Electron Devices* 40 (1993) 1754-1759.
- [44] A. Berns, U. Buder, E. Obermeier, A. Wolter, A. Leder, AeroMEMS sensor array for high-resolution wall pressure measurements, *Sensors and Actuators A: Physical* 132 (2006) 104-111.
- [45] C.H. Je, S.Q. Lee, W.S. Yang, High Sensitivity Surface Micromachined Absolute Pressure Sensor, *Procedia Engineering* 168 (2016) 725-728.
- [46] S. Guo, H. Eriksen, K. Childress, A. Fink, M. Hoffman, High temperature smart-cut SOI pressure sensor, *Sensors and Actuators A: Physical* 154 (2009) 255-260.
- [47] Y. Hamid, D.A. Hutt, D.C. Whalley, R. Craddock, Relative contributions of packaging elements to the thermal hysteresis of a MEMS pressure sensor, *Sensors* 2020.
- [48] Å. Sandvand, E. Halvorsen, K. E. Aasmundtveit, H. Jakobsen, Identification and Elimination of Hygro-Thermo- Mechanical Stress-Effects in a High-Precision MEMS Pressure Sensor, *Journal of Microelectromechanical Systems*, 26 (2017) 415-423.
- [49] K. Birkelund, P. Gravesen, S. Shiryaev, P. B. Rasmussen, M. D. Rasmussen, High-pressure silicon sensor with low-cost packaging, *Sensors and Actuators A: Physical* 92 (2001) 16-22.
- [50] L. Christel, K. Petersen, P. Barth, F. Pourahmadi, J. Mallon, J. Bryzek, Single-crystal Silicon Pressure Sensors with 500x Overpressure Protection, *Sensors and Actuators A: Physical* A21-A23 (1990) 84-88.
- [51] D.M. Prigodskiy, M.V. Basov, Research of Pressure Sensitive Elements with Increased Strength, *Nano- and Microsystem Technology*, Nano- and Microsystem Technology 6 (2019) 368-376.

- [52] T. Kober, R. Werthschützky, Wafer Level Processing of Overload-Resistant Pressure Sensors, *Procedia Engineering* 47 (2012) 615-618.



Mikhail Basov graduated in 2012 from National Nuclear Research University "Moscow Engineering Physics Institute" (department of Nano- and Microelectronics). Starting from 2010 he works as R&D engineer on advanced MEMS pressure sensing elements. His Ph.D. thesis is titled "High-Sensitivity Pressure Sensor Chip Utilizing Bipolar-Junction Transistors". He won the award of state atomic energy corporation Rosatom with project "Ultra-High Sensitive Pressure Sensor with Increased Strength" in 2019.

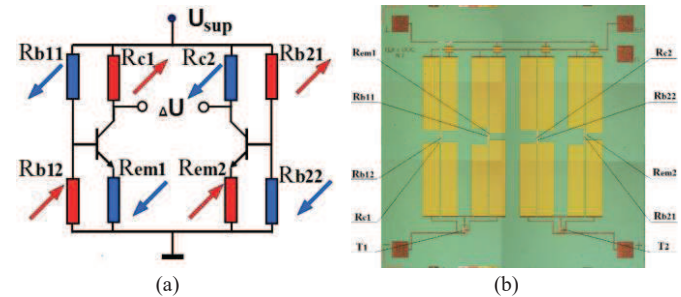


Fig. 1. Ultra-high sensitivity pressure sensor PDA-NFL: a) electrical circuit, b) top view of chip.

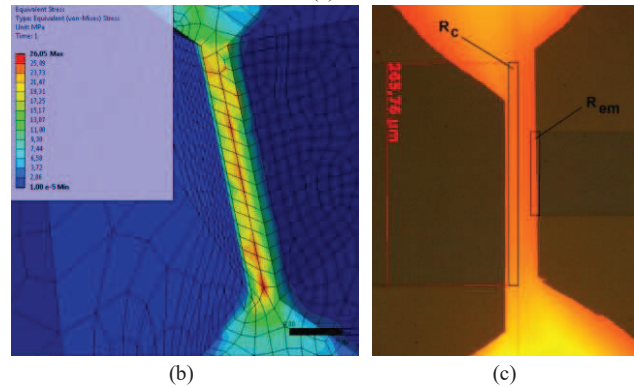
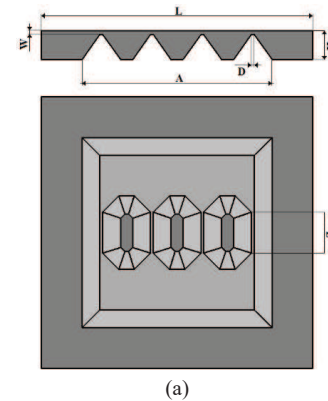


Fig. 2. Membrane of ultra-high sensitivity pressure sensor chip PDA-NFL: a) structure overview, b) distribution of the mechanical stress (von Mises) between R1, c) photo of the area between R1.

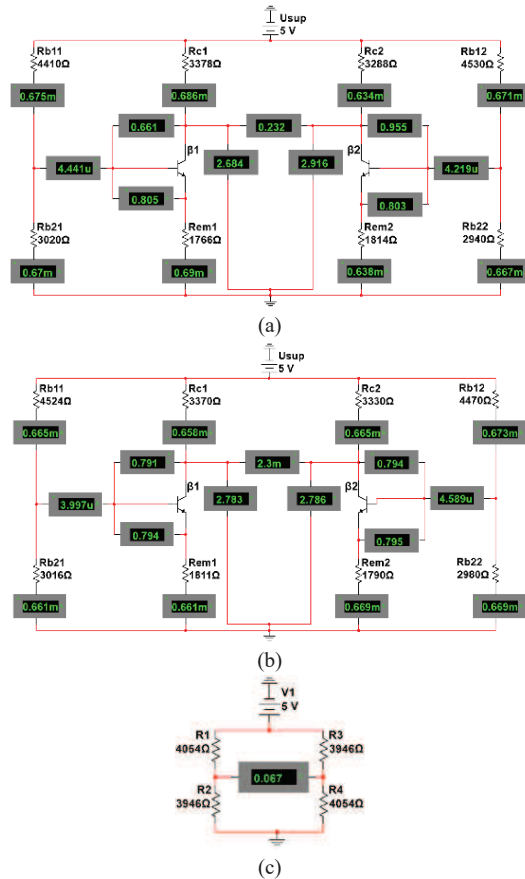


Fig. 3. Parameters of PDA-NFL circuit calculated in NI Multisim on: pressure (a) and temperature (b); parameters of Wheatstone bridge circuit calculated in NI Multisim on pressure (c).

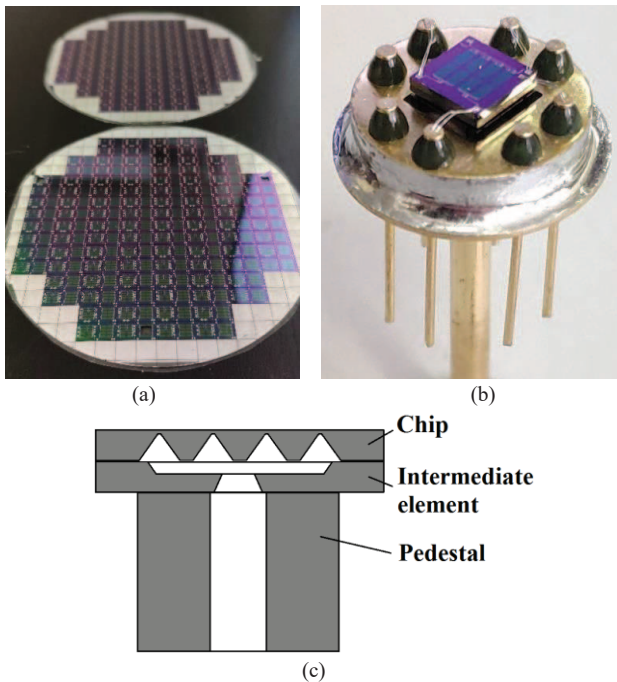


Fig. 4. Ultra-high sensitivity pressure sensor chip PDA-NFL: a) final view of chip on the wafers, b) view of pressure sensor (without gap for case), c) silicon structure for connecting chip with case.

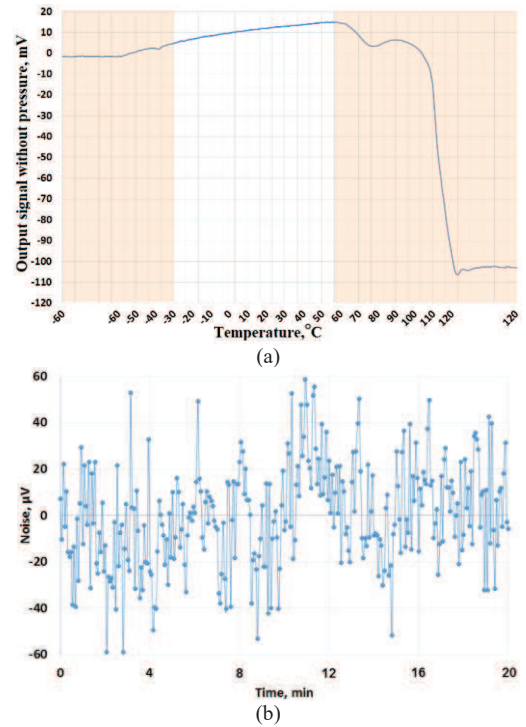


Fig. 5. Dependence of zero output signal on temperature (a) and time (b) for sample of PDA-NFL chip.

TABLE I

GEOMETRICAL PARAMETERS OF MEMBRANE FOR ULTRA-HIGH SENSITIVITY PRESSURE SENSOR CHIP PDA-NFL

Geometrical Parameters	Size, μm
L	4000 ± 50
W	9 ± 2
H	400 ± 5
A	2810 ± 15
D	39 ± 5
Z	270 ± 50

TABLE II

MODELED PARAMETERS OF ULTRA-HIGH SENSITIVITY PRESSURE SENSOR CHIP PDA-NFL

Elements	Parameters	Value
Common	Supply voltage U_{sup} , V	5
	Base current I_b , μA	4.6
	Gain β	145
BJT	Base-emitter voltage ($U_b - U_{\text{em}}$), V	0.80
	Base-collector voltage ($U_c - U_b$), V	0.80
PR	Collector potential U_c , V	2.79
	$R_{b11, b21}$, kOhm	4.47
	$R_{b12, B22}$, kOhm	2.98
	$R_{c1, c2}$, kOhm	3.33
	$R_{em1, em2}$, kOhm	1.79
Sensitivity S, mV/V/kPa		46.4
Additional component of temperature coefficient of zero TCZ, %FS/°C		0.099

TABLE III

DIFFUSION PARAMETERS OF ULTRA-HIGH SENSITIVITY PRESSURE SENSOR CHIP PDA-NFL

Process step	Methods
Oxidation	1100 °C, 15 min – 20 min – 15 min (dry-wet-dry)
High-doped p ⁺ areas of isolation BJTs	Diffusion from unlimited source: 1050 °C, 55 min. Drive-in and oxidation: 1200 °C, 330 min (dry)
High-doped p ⁺ areas of PRs	Diffusion from unlimited source: 1050 °C, 55 min. Drive-in and oxidation: 1150 °C, 5 min – 15 min – 5 min (dry-wet-dry)
Low-doped p ⁻ areas of PRs, base of V-NPN transistor	Ion implantation: $D = 8.0 \cdot 10^{14} \text{ cm}^{-2}$, $E = 50 \text{ keV}$ Impurity activation and oxidation: 1100 °C for 45 min in inert atmosphere followed by oxidation 1000 °C, 5 min – 35 min – 5 min. (dry-wet-dry)
High-doped n ⁺ collector (ohmic contact) and emitter of V-NPN transistor	Ion implantation: $D = 10.4 \cdot 10^{15} \text{ cm}^{-2}$, $E = 70 \text{ keV}$ Impurity activation and oxidation: 1030 °C, 25 min in inert atmosphere followed by oxidation 1030 °C, 5 min – 45 min – 5 min (dry-wet-dry)

TABLE IV

PERFORMANCE OF ULTRA-HIGH SENSITIVITY PRESSURE SENSOR CHIP PDA-NFL

Parameters	PDA-NFL (V-NPN)
Sensitivity, mV/V/kPa	44,9 ± 8,8
Zero pressure output signal (Offset), mV/V	< 20
Average noise voltage, μV/V	12
Nonlinearity, $2K_{NL}$, %FS	1,20 ± 0,31
Thermal coefficient of zero	(-30...+20 °C), %FS/°C (+20...+60 °C), %FS/°C 0,092 ± 0,055 0,096 ± 0,030
Thermal coefficient of span	(-30...+20 °C), %FS/°C (+20...+60 °C), %FS/°C 0,633 ± 0,175 0,634 ± 0,193
Thermal hysteresis of zero	(-30...+20°C), %FS (+20...+60°C), %FS 0,341 ± 0,202 0,262 ± 0,152
Thermal hysteresis of span	(-30...+20°C), %FS (+20...+60°C), %FS 0,611 ± 0,173 0,343 ± 0,260
Long-term stability (Drift)	of zero offset, %FS of pressure sensitivity, %FS 0,12 ± 0,11 0,17 ± 0,12
Burst pressure, kPa	> 550
Zero changing after proof pressure	from top side from bottom side 0,08 ± 0,09 0,06 ± 0,05
Zero change after flipping sensor in gravity field, μV	64 ± 21
Number of samples in statistics	14